ADVANCED MATERIALS
www.advmat.de

Ultracoherent Single-Electron Emission of Carbon Nanotubes

Aiwei Wang, Jiuzhou Zhao, Ke Chen, Zhenjun Li, Chi Li, and Qing Dai**

A single-electron emitter, based on a single quantized energy level, can potentially achieve ultimate temporal and spatial coherence with a large emission current, which is desirable for atomic-resolution electron probes. This is first developed by constructing a nano-object on a metal tip to form a quantized double barrier structure. However, the single-electron-emission current can only achieve a picoampere level due to the low electron tunneling rate of the heterojunction with large barrier width, which limits the practical applications. In this study, carbon nanotubes (CNTs) serve as a single-electron emitter and a current up to 1.5 nA is demonstrated. The double barrier structure formed on the CNT tip enables a high tunneling rate (≈10^{12} s^{-1}) due to the smaller barrier width. The emitter also shows high temporal coherence (energy dispersion of ≈10 meV) and spatial coherence (effective source radius of ≈0.85 nm). This work represents a highly coherent electron source to simplify the electron optics system of atomic-resolution electron microscopy and sub-10 nm electron beam lithography.

1. Introduction

Cold field-emission electron sources that rely on metal nanotips have generated significant interest due to their small virtual source sizes (≈10 nm) and relatively narrow energy spreads (<500 meV).[1] However, a much narrower energy spread (<50 meV) is required for achieving atomic-level resolution electron probe and high energy-resolution electron energy loss spectroscopy.[2–5] Unfortunately, further reducing the energy spread of conventional metal nanotips is a significant challenge, due to the broadening of the initial emitting energy level and the Coulomb interaction of emitted electrons. Presently, one solution involves equipping a monochromator in the state-of-the-art high-resolution transmission electron microscope.[2,4] However, this setup dramatically reduces the probe current to a picoampere level, which significantly reduces the signal-to-noise ratio and spatial resolution.[3,4,6] Therefore, a new field emitter with a narrower energy spread and higher emission current must be developed to break through this bottleneck.

Single-electron emission through a single quantized energy level is the ultimate model to overcome the abovementioned challenge, which can be realized through resonant tunneling field emission in a Coulomb blockade regime.[7–12] In this model, the initial emission is primarily confined within an ultranarrow energy level.[7,8,12] Moreover, the Coulomb interaction between electrons can be avoided as emitted electrons are well-separated in time.[8,12–14] This model relies on a double barrier sandwiched quantum dot or potential well structure (i.e., quantized double barrier structure), which can be achieved by constructing a nano-object on metal nanotip.[7–9,15] However, achieving a high emission current (>1 nA) in a single-electron emission regime is challenging, because the tunneling rate of the heterojunction barrier between the nano-object and the metal nanotip is relatively low due to its large width. A tip of a 1D carbon nanotube (CNT) is a potential structure for this purpose.[8,12,16,17] First, homojunction double barrier structures have been proven to be naturally formed at the tip of CNTs, which might enable a larger electron tunneling rate.[16,17] Second, a high brightness of up to 10^{11} A str^{-1} m^{-2} V^{-1} is achievable due to the robust mechanical structure and electrical conductivity.[18] Last, the weak interaction of low-energy electrons with both optical and acoustic phonons enables ballistic transport, which significantly limits electron scattering.[19]

In this study, we demonstrate the formation of a double barrier structure on a CNT tip at cryogenic temperatures ranging from 10 to 160 K. Our results show a distinctive staircase-like field-emission curve with equidistant conductance peaks, indicating an energy level renormalization as a result of Coulomb blockade effect. This observation suggests that emission from a single quantized energy level is in a single-electron regime. The conductance peaks exhibit a good fit to a Lorentzian line, implying quasi-perfect resonant tunneling field emission. Thanks to the large tunneling rate (≈10^{12} s^{-1}) double barrier structure possibly induced by the small barrier width, we were able to obtain a high emission current of ≈1.5 nA from a single quantized energy level with an estimated width of ≈10 meV. Additionally, we

A. Wang, J. Zhao, K. Chen, Z. Li, C. Li, Q. Dai
CAS Key Laboratory of Nanophotonic Materials and Devices, CAS Key Laboratory of Standardization and Measurement for Nanotechnology, CAS Center for Excellence in Nanoscience
National Center for Nanoscience and Technology
Beijing 100190, P. R. China
E-mail: lichi@nanoctr.cn; daiq@nanoctr.cn
A. Wang, J. Zhao, K. Chen, Z. Li, C. Li, Q. Dai
Center of Materials Science and Optoelectronics Engineering
University of Chinese Academy of Sciences
Beijing 100049, P. R. China

The ORCID identification number(s) for the author(s) of this article can be found under https://doi.org/10.1002/adma.202300185

DOI: 10.1002/adma.202300185

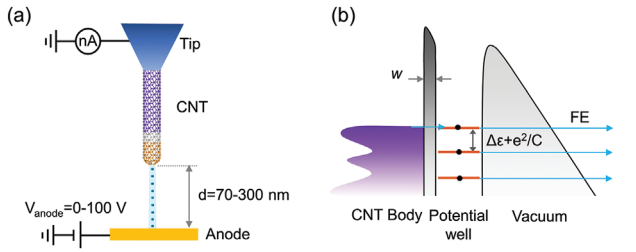

Figure 1. The schematic diagram of the experimental setup and the double barrier model of the CNT emitter. a) Schematic diagram of the experimental setup. The CNT is grown on the apex of a tungsten tip. The emission distance (d) between the emitter and the anode is controlled by the STM feedback system, which is from ≈70 nm to a few hundred nanometers. b) The model of the double barrier structure. A double barrier structure is formed at the apex of a CNT with w the contact barrier width between the potential well and the CNT reservoir. The blue arrow indicates the electron transport path.

measured the effective source radius to be ≈0.85 nm. Overall, our work provides crucial material fundamentals and design principles for the development of high-brightness coherent single-electron sources for atomic-resolution electron microscopy and electron beam lithography.

2. Results and Discussion

To assess the field-emission properties, we employed a scanning tunneling microscope (STM) with a pressure of 3×10^{-10} Torr and a temperature range of 10–300 K. Figure 1a illustrates the experimental setup, in which several multi-walled CNTs, ranging in length from several micrometers and with a diameter of ≈10 nm, were grown directly on the apex of a sharp tungsten tip (see Figure S1, Supporting Information for details). An anode made of a single-crystal Au (111) was positively biased by a voltage ranging from 0 to 100 V. The STM feedback system controlled the emission distance between the emitter and anode (see Figure S2, Supporting Information for details). A cyclic aging procedure was performed until a stable field emission was achieved, characterized by a highly repeatable staircase-like feature (See Figure S3, Supporting Information for details). This ensured that the emission occurs from a single CNT tip, as discussed below. The presence of a typical double barrier structure is shown in Figure 1b.

Figure 2a exhibits a typical staircase-like field-emission curve, with the inset showing the corresponding Fowler–Nordheim (FN) plot. Given the work function of CNT as ≈5 eV, the field enhancement factor is calculated as $\beta \approx 7$ (see Figure S4, Supporting Information for details).[20] This value is smaller than normal CNT enhancement factors, which is mainly due to the ultrashort emission distance.[21–23] Figure 2b shows the corresponding differential conductance curve in Figure 2a. More than nine equidistant differential conductance peaks are observed in intervals (ΔV) of ≈1 V with peak height varying from peak to peak, which indicates the behavior of Coulomb blockade-mediated field emission through quantized energy levels in a quantum structure (QS).[12,14,24] The equidistant peaks have resulted from the renormalized equidistant energy levels, which are mediated by the charging effect. The energy spacing is determined by $\Delta E = \Delta\varepsilon + (C/e^2)$ where $\Delta\epsilon$ is intrinsic level spacing in the QS, e is the elementary charge, and C is the capacitance of the QS.[12,14,24] The peak heights are determined by the width of the levels.[11,25] While the presence of two or more nanotubes with varied lengths contributing to emissions may also create distinct features in the emission curve, it is not likely to produce a step-like feature due to the monotonically increasing nature of the FN field-emission curve. As a result, we would observe a monotonically increasing conductance curve rather than a series of peaks in the differential conductance curve. Therefore, our observations confirm the occurrence of field emission through quantized energy levels of a single CNT within the Coulomb blockade regime.

Next, we investigated the tunneling behavior. As shown in Figure 2c, the normalized conductance peaks have Lorentzian line shapes, indicating that the sharp conductance peak originates from resonant tunneling through a single quantized energy level in a double barrier structure.[7,8,11,26] The R^2 values of the Lorentzian fitting are close to 1, suggesting a quasi-perfect resonance. The full width at half maximum (FWHM) of the peak is 70 mV according to the Lorentzian fitting. In addition, as depicted in Figure 2d, the peaks generally broaden as the emission current increases due to thermal broadening caused by the Joule heating effect from the emission current.[8,27] However, noteworthy is that both the FWHM and peak height generally decrease from the third to the fourth peak. Such non-monotonic behavior indicates that the peak width is mainly shaped by the intrinsic energy level width, rather than the thermal broadening energy of ≈1 meV at 10 K. The considerably wide energy level width largely minimized the thermal deterioration of electron resonance in the cavity and thus guaranteed a quasi-perfect resonant tunneling current.[8]

The emitting energy level width can be estimated according to the principle illustrated in Figure S4 (Supporting Information). First, the energy spacing of two adjacent energy levels is determined by $\Delta E = ew\Delta F = e\Delta V/\eta$, where $\eta \approx d/\beta w$, with β the field enhancement factor and w the internal barrier width.[28,29] The validity of this formula is confirmed by the emitter–anode distance-dependent I–V curve (Figure S4a, Supporting Information), in which the staircases occur at a fixed emission current value independent of the bias voltage. The β value obtained in Figure 2a is further confirmed by finite element method calculations and η can be approximately estimated to be 10 (see Figure S4, Supporting Information). Thus, the 1V peak interval corresponds to an energy spacing of ≈100 meV and the 70 mV FWHM corresponds to the intrinsic level width of ≈7 meV. The level width is much larger than those in the previously reported Coulomb blockade-resonant tunneling cases, which also corresponds to a large tunneling rate of $\approx 10^{12}$ s^{-1}.[7,8,11]

The possible origin of the internal barrier can be analyzed from the discussion above. As illustrated in the inset of Figure 2b, the spacing between the peaks progressively decreases as the bias voltage increases from the first to the third peak. This indicates that the QS capacitance, determined by its size, is increasing. Therefore, the size-tunable QS is very likely the electric field-induced inversion region of the semiconducting CNT, while the internal barrier is the depletion barrier. Due to the p-type semiconducting nature of as-grown multiwall CNTs, a nanoscale inversion region (n-type) as the QS will be induced at the tip.[30] At low bias voltage, the thickness of the inversion region increases

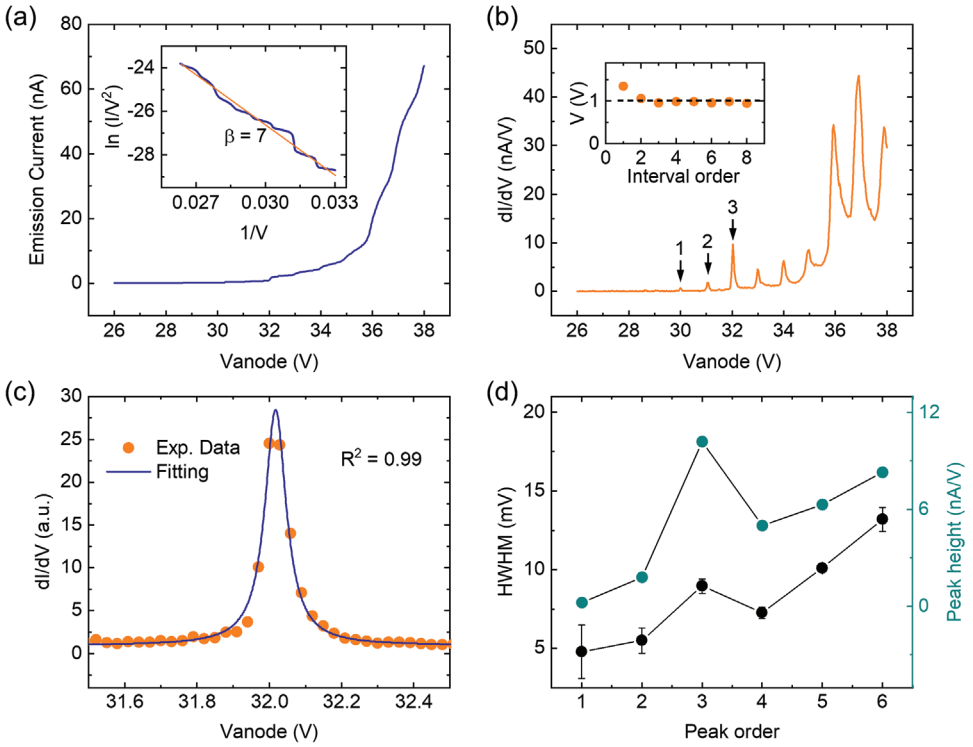

Figure 2. The resonant tunneling field emission in the Coulomb blockade regime. a) The field-emission curve (*I*–*V* curve) was obtained at a voltage setpoint, V_{setset} = 32 V and a current setpoint, $I_{set\ set}$ = 1 nA, under 10 K temperature. The inset is the FN plot of the emission curve, which is linearly fitted, indicated by the red line. The staircase-like features appear in both *I*–*V* and FN curves. b) The differential conductance curve from the field-emission curve. Conductance peaks correspond to the staircases in the field-emission curve. The peak orders are marked in the figure. The inset is the peak interval (Δ*V*) between the different peaks. c) Blue Lorentzian fitting line of the normalized conductance peak corresponding to peak 3. d) Dependence of the FWHMs and the peak heights with respect to the increase in the peak order.

with the voltage increases. When the inversion region's thickness is sufficiently large, with a significant electron density, the external electric field is screened, and the inversion region size becomes saturated. Thus, the peak spacing no longer increases after the third peak. Although other factors, such as defects between CNT fragments[16] and nano protrusions at the apex of the CNT,[31] could also contribute to the internal barrier's formation, the depletion barrier appears to be the most likely cause. Considering the homojunction essence of the double barrier structure at the CNT tip, the internal barrier width is possibly small, enabling a high tunneling rate.

Let us now discuss the practical applications in electron sources of the CNT field emission. Figure 3a shows the typical field emission and differential conductance curves of various samples obtained at temperatures of 25, 160, and 300 K. As the temperature increases, the curves become less

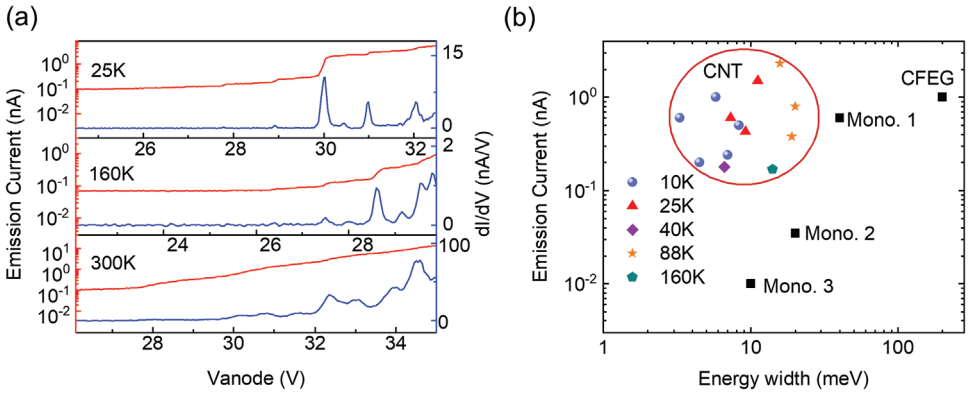

Figure 3. The high-temperature properties of the resonant tunneling field emission. a) Field-emission curve and the differential conductance curves were obtained at 25, 160, and 300 K with V_{setset} = 30 V and I_{setset} = 1 nA. b) Comparison of the beam current and the energy spread from this study, the state-of-the-art electron-source-like cold field-emission gun,[32] and the STEM monochromated electron source (Mono.1,[4] 2,[33] 3[3]).

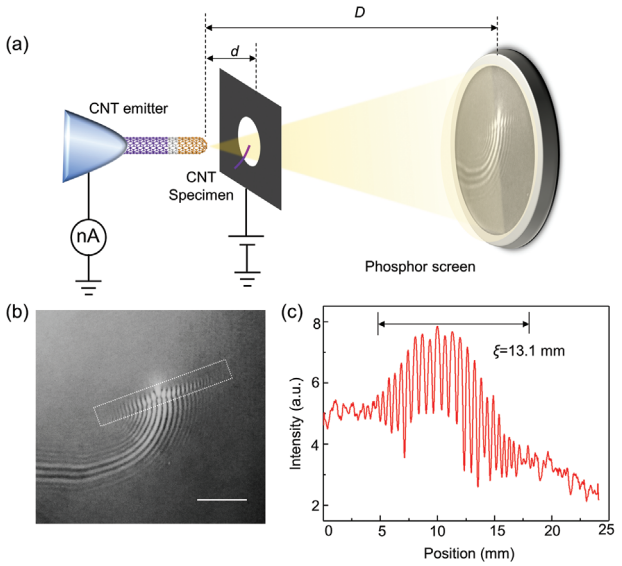

Figure 4. The offline holography of the CNT electron source under room temperature. a) Experimental holography setup. Another CNT is put onto a gold grid as a biprism. The electron energy is 200 eV. b) Electron interference fringes on the screen. Scale bar: 5 mm. c) The line profile of the interference fringes in(b) enclosed in the rectangle.

distinguishable, and the conductance peaks tend to merge due to increasing thermal broadenings. The R^2 values of the Lorentzian fitting of the discrete conductance peaks are close to 1 in a wide temperature range from 10 to 160 K (see Section 5 in the Supporting Information). Figure 3b shows the distribution of the level widths and the current rise of the corresponding resonance peaks of different samples under five different temperatures. The present CNT emitters provide ≈1.5 nA through a narrow energy width of ≈10 meV, as shown in the top panel in Figure 3b. In comparison, the monochromatic electron sources obtained in the state-of-the-art monochromator in a scanning transmission electron microscope (STEM) are shown as Mono.1–3 in Figure 3b. A probe current of 600, 35, or 10 pA can be reached when the energy spread is 40, 20, or 10 meV, respectively.[3,4] Meanwhile, for a cold field-emission gun with a monochromator, a probe current can reach 1 nA, while the energy spread can be as large as 200 meV. Therefore, our CNT emitters may enhance the brightness of atomic-scale electron probes by more than two orders with lower energy spread.

Lastly, the spatial coherence of electrons emitted from the CNT is measured using a point projection microscope at room temperature, as illustrated in Figure 4a.[34,35] A second CNT with a diameter of ≈10 nm was used as a biprism, positioned close to the emitting tip with a distance of ≈1 μm. A microchannel plate and a phosphor screen are positioned 400 mm away from the emitter. As depicted in Figure 4b, a clear image of the CNT was obtained, displaying sharp interference fringes. The virtual source size was calculated using the formula $r = \lambda D/\pi\xi$, where the$\lambda$is electron beam wavelength, D is the distance between the tip and the screen, and ξ is transverse coherence length of the electron beam.[34,35] ξ was 13.1 mm according to the measured interference fringes (Figure 4c). The resulting calculated virtual source size was ≈0.85 nm, indicating a single CNT-based electron source with high spatial coherence.

3. Conclusion

We have demonstrated the formation of a double barrier structure on a CNT tip, evidenced by a distinctive staircase-like field-emission curve with equidistant conductance peaks. A high-tunneling-rate (≈10^{12} s^{-1}) resonant-type field emission in the Coulomb blockade regime is achieved possibly due to the small barrier width, enabling the single-electron-emission current to reach as high as 1.5 nA. Furthermore, the high temporal and spatial coherence of the electrons are respectively demonstrated by the low energy spread of ≈10 meV and the small effective source radius of ≈0.85 nm. Our findings pave the way toward atomic-resolution electron probes for high-resolution microscopy and electron beam lithography. Further optimization of structural parameters, such as reducing the internal barrier width by changing the charity of the CNT, can lead to a larger tunneling rate and thus a larger emission current.

Supporting Information

Supporting Information is available from the Wiley Online Library or from the author.

Acknowledgements

The authors acknowledge funding from the Natural Science Foundation of China (51972072, 52072084, 52025023, 52222207),the Key Area Research and Development Program of Guangdong Province (Grant No. 2020B0101020002), and the GBA National Institute for Nanotechnology Innovation (Grant No. 2020GN0106).

Conflict of Interest

The authors declare no conflict of interest.

Author Contributions

A.W.W. and J.Z.Z. contributed equally to this work. Q.D. and C.L. conceived the experiments. A.W.W. and J.Z.Z. prepared the as-grown samples and performed experiments. A.W.W. and C.L. analyzed the data and organized the figures. Q.D., C.L., A.W.W. and J.Z.Z. cowrote the paper. All authors discussed the results and commented on the paper.

Data Availability Statement

The data that support the findings of this study are available from the corresponding author upon reasonable request.

Keywords

coherent electron sources, field emission, resonant tunneling, single-electron emission

Received: January 6, 2023
Revised: April 5, 2023
Published online: June 27, 2023

[1] T. Kawasaki, T. Akashi, K. Kasuya, H. Shinada, *Ultramicroscopy* **2019**, *202*, 107.
[2] H. W. Mook, P. Kruit, *Ultramicroscopy* **1999**, *78*, 43.
[3] O. L. Krivanek, T. C. Lovejoy, N. Dellby, T. Aoki, R. W. Carpenter, P. Rez, E. Soignard, J. T. Zhu, P. E. Batson, M. J. Lagos, R. F. Egerton, P. A. Crozier, *Nature* **2014**, *514*, 209.
[4] S. Lopatin, B. Cheng, W. T. Liu, M. L. Tsai, J. H. He, A. Chuvilin, *Ultramicroscopy* **2018**, *184*, 109.
[5] N. Li, X. D. Guo, X. X. Yang, R. S. Qi, T. Y. Qiao, Y. F. Li, R. C. Shi, Y. H. Li, K. H. Liu, Z. Xu, L. Liu, F. J. García de Abajo, Q. Dai, E. G. Wang, P. Gao, *Nat. Mater.* **2021**, *20*, 43.
[6] K. Kimoto, *Microscopy* **2014**, *63*, 337.
[7] N. C. van der Vaart, S. F. Godijn, Y. V. Nazarov, C. J. Harmans, J. E. Mooij, L. W. Molenkamp, C. T. Foxon, *Phys. Rev. Lett.* **1995**, *74*, 4702.
[8] E. B. Foxman, P. L. Mceuen, U. Meirav, N. S. Wingreen, Y. Meir, P. A. Belk, N. R. Belk, M. A. Kastner, S. J. Wind, *Phys. Rev. B* **1993**, *47*, 10020.
[9] T. Esat, N. Friedrich, F. S. Tautz, R. Temirov, *Nature* **2018**, *558*, 573.
[10] V. I. Kleshch, V. Porshyn, D. Lutzenkirchen-Hecht, A. N. Obraztsov, *Phys. Rev. B* **2020**, *102*, 235437.
[11] C. W. J. Beenakker, *Phys. Rev. B* **1991**, *44*, 1646.
[12] M. Bockrath, D. H. Cobden, P. L. McEuen, N. G. Chopra, A. Zettl, A. Thess, R. E. Smalley, *Science* **1997**, *275*, 1922.
[13] L. Cockins, Y. Miyahara, S. D. Bennett, A. A. Clerk, S. Studenikin, P. Poole, A. Sachrajda, P. Grutter, *Proc. Natl. Acad. Sci. USA* **2010**, *107*, 9496.
[14] L. P. Kouwenhoven, D. G. Austing, S. Tarucha, *Rep. Prog. Phys.* **2001**, *64*, 701.
[15] M. Duchet, S. Perisanu, S. T. Purcell, E. Constant, V. Loriot, H. Yanagisawa, M. F. Kling, F. Lepine, A. Ayari, *ACS Photonics* **2021**, *8*, 505.
[16] S. T. Purcell, P. Vincent, M. Rodriguez, C. Journet, S. Vignoli, D. Guillot, A. Ayari, *Chem. Vap. Deposition* **2006**, *12*, 331.
[17] M. J. Fransen, T. L. van Rooy, P. Kruit, *Appl. Surf. Sci.* **1999**, *146*, 312.
[18] A. Pascale-Hamri, S. Perisanu, A. Derouet, C. Journet, P. Vincent, A. Ayari, S. T. Purcell, *Phys. Rev. Lett.* **2014**, *112*, 126805.
[19] P. Poncharal, C. Berger, Y. Yi, Z. L. Wang, W. A. de Heer, *J. Phys. Chem. B* **2002**, *106*, 12104.
[20] N. de Jonge, M. Allioux, M. Doytcheva, M. Kaiser, K. B. K. Teo, R. G. Lacerda, W. I. Milne, *Appl. Phys. Lett.* **2004**, *85*, 1607.
[21] C. He, W. Wang, S. Deng, N. Xu, Z. Li, *J. Phys. Chem. A* **2009**, *113*, 7048.
[22] M. Passacantando, F. Bussolotti, S. Santucci, A. Di Bartolomeo, F. Giubileo, L. Iemmo, A. M. Cucolo, *Nanotechnology* **2008**, *19*, 395701.
[23] R. C. Smith, J. D. Carey, R. D. Forrest, S. R. P. Silva, *J. Vac. Sci. Technol., B: Microelectron. Nanometer Struct.–Process., Meas., Phenom.* **2005**, *23*, 632.
[24] L. A. Ponomarenko, F. Schedin, M. I. Katsnelson, R. Yang, E. W. Hill, K. S. Novoselov, A. K. Geim, *Science* **2008**, *320*, 356.
[25] M. L. Perrin, E. Burzuri, H. S. J. van der Zant, *Chem. Soc. Rev.* **2015**, *44*, 902.
[26] I. J. Maasilta, V. J. Goldman, *Phys. Rev. B* **1997**, *55*, 4081.
[27] L. Jdira, K. Overgaag, R. Stiufiuc, B. Grandidier, C. Delerue, S. Speller, D. Vanmaekelbergh, *Phys. Rev. B* **2008**, *77*, 205308.
[28] L. Jdira, P. Liljeroth, E. Stoffels, D. Vanmaekelbergh, S. Speller, *Phys. Rev. B* **2006**, *73*, 115305.
[29] P. Liljeroth, P. A. Zeijlmans van Emmichoven, S. G. Hickey, H. Weller, B. Grandidier, G. Allan, D. Vanmaekelbergh, *Phys. Rev. Lett.* **2005**, *95*, 086801.
[30] J. Park, P. L. McEuen, *Appl. Phys. Lett.* **2001**, *79*, 1363.
[31] V. I. Kleshch, V. Porshyn, P. Serbun, A. S. Orekhov, R. R. Ismagilov, S. A. Malykhin, V. A. Eremina, P. A. Obraztsov, E. D. Obraztsova, D. Lutzenkirchen-Hecht, *Appl. Phys. Lett.* **2021**, *118*, 053101.
[32] J. M. Zuo, J. C. H. Spence, *Advanced Transmission Electron Microscopy*, Springer, New York **2017**.
[33] L. H. Tizei, Y. C. Lin, M. Mukai, H. Sawada, A. Y. Lu, L. J. Li, K. Kimoto, K. Suenaga, *Phys. Rev. Lett.* **2015**, *114*, 107601.
[34] J. Vogelsang, N. Talebi, G. Hergert, A. Woste, P. Gross, A. Hartschuh, C. Lienau, *ACS Photonics* **2018**, *5*, 3584.
[35] D. Ehberger, J. Hammer, M. Eisele, M. Kruger, J. Noe, A. Hogele, P. Hommelhoff, *Phys. Rev. Lett.* **2015**, *114*, 255501.